J Solid State Electrochem (2012) 16:1733–1739
DOI 10.1007/s10008-011-1600-8

ORIGINAL PAPER

Fabrication of nano-network gold films via anodization of gold electrode and their application in SERS

Yingchang Yang · Yue Xia · Wei Huang · Jufang Zheng · Zelin Li

Received: 3 August 2011 / Revised: 3 November 2011 / Accepted: 14 November 2011 / Published online: 25 November 2011

Abstract We report here a green and facile one-step method to fabricate nano-network gold films of low roughness via anodization of gold electrodes in an aqueous solution of L-ascorbic acid (AA) or hydroquinone (H_2Q) at the oxidation peak potential. The preparation involves the formation of thin gold oxide layer by anodization of gold and its simultaneous and/or subsequent reduction by AA or H_2Q. The as-fabricated nano-network gold films show very strong SERS activity in comparison with the substrates prepared by some other electrochemical roughening methods.

Keywords Nano-network · Gold anodization · Ascorbic acid · Hydroquinone · SERS

Introduction

Gold nanostructures have been attracting increasing interest for their wide applications in areas such as catalysis [1], biosensors [2], fuel cells [3], surface-enhanced Raman scattering (SERS) [4], and so on. In particular, gold electrode surfaces roughened by electrochemical approaches are commonly used as SERS active substrates, which are especially suitable for potential-dependent electrochemical SERS investigation [5].

Up to present, a number of electrochemical strategies have been developed for fabricating nanostructured gold electrodes for SERS substrates, including roughening gold electrodes with triangular-wave electrochemical oxidation reduction cycles (ORC) [6, 7], anodic potential step [8–10] and square-wave potential-pulses [11], and templated electrodeposition [12]. Recently, a nanoporous gold film with thickness of approximately 1 μm was made by anodization of gold electrode in an aqueous solution of carboxylic acid or carboxylate [13, 14]. SERS activity was closely correlative to the nanostructures rather than to the roughness factor [12, 15].

Herein, we present a green and facile one-step method to fabricate nano-network gold films of low roughness via anodization of gold in a solution of L-ascorbic acid (AA). AA is the only nontoxic and inexpensive agent employed in this process. The as-fabricated nano-network gold films possess very strong SERS activity in comparison with the substrates prepared by some other electrochemical roughening methods. Another reductant, hydroquinone (H_2Q), has also been investigated. To our knowledge, no such work has been reported on the fabrication of low-roughness nano-network surface by anodization of gold in the presence of reductants for SERS.

Experimental section

Reagents and electrodes

All reagents were of analytical grade and were used without further purification, and all solutions were prepared using

Y. Yang · Y. Xia · W. Huang · Z. Li (✉)
Key Laboratory of Chemical Biology and Traditional Chinese Medicine Research (Ministry of Education of China),
College of Chemistry and Chemical Engineering,
Hunan Normal University,
Lushan Road,
Changsha 410081, China
e-mail: lizelin@hunnu.edu.cn

J. Zheng
Key Laboratory of the Ministry of Education for Advanced Catalysis Materials, Institute of Physical Chemistry,
Zhejiang Normal University,
Jinhua 321004, China

high-purity water from a Milli-Q water purification system (Millipore Corp., USA).

A 1-mm-diameter polycrystalline gold disk electrode (purity >99.99%), a circular platinum wire, and a saturated mercurous sulfate electrode (SMSE) were employed as the working, counter, and reference electrode, respectively. Electrochemical and Raman measurements were all carried out in a self-made spectroscopic cell with a quartz window [5]. All potentials quoted here are vs. SMSE.

Fabrication and characterization of nano-network gold films

Electrochemical experiments were performed with a CHI 660 C electrochemical station (Chenhua, Shanghai, China). The gold working electrode was polished using finer grades of emery paper and alumina powder down to 0.05 μm, followed by ultrasonic cleaning in ultrapure water. To obtain reproducible results, the roughness factor of gold electrode after polishing should be nearly 3. Then, the gold electrode was roughened in 0.5 M AA (or 0.06 M H_2Q) with an applied potential of 1.2 V (or 1.5 V) for different times.

For comparison, gold electrodes were also roughened by potential step [16] and ORC [7]. In potential step, the electrode was immersed in 2 MHCl and the potential was stepped from open-circuit potential to 0.9 V for 50 s. In ORC, the electrode was cycled in 0.1 M KCl aqueous solution from −0.7 to+0.8 V for 25 scans. The durations at the cathodic and anodic vertexes were 30 and 1.3 s, respectively.

The morphologies of gold electrodes were characterized by a Hitachi S-4800 field-emission scanning electron microscope (SEM) with an electron beam voltage of 5 kV. The surface chemical states of the nano-network gold films were analyzed with an ESCALab250 X-ray photoelectron spectroscope.

SERS measurements

Raman spectra were obtained on a Renishaw RM1000 confocal Raman spectrometer (Renishaw Inc., New Mills, UK) with 633-nm excitation operating at 1% power (ca. 0.14 mW). A 50× long-working-length objective was used to focus laser light on the electrode in an aqueous solution containing 0.1 M KCl and 0.01 M Py. Raman measurement was started after 3 min of waiting time in order to stabilize the conditions. Each Raman spectrum is an average of five replicate measurements collected from different surface areas with acquisition time of 10 s for each sample.

Results and discussions

Fabrication of nano-network gold films

Figure 1a shows typical linear sweep voltammetry (LSV) of the polished gold electrode in 0.5 M AA. When the potential was swept from −0.5 to 1.8 V (versus SMSE) at a rate of 100 mV s^{-1}, the anodic current appeared at −0.25 V, increased rapidly, and then decreased considerably as the potential was positive to 1.2 V. We observed that blackening occurred on the gold surface when holding the potential at the peak of 1.2 V. However, no blackening was observed on the gold surface below 1.0 V or above 1.3 V. These results imply that 1.2 V is an appropriate choice to roughen the gold electrode surface in the solution of AA. Apparently, in the above potential sweep range, the LSV curve comprises complicated reactions, like oxidation of AA, formation of gold oxides, and reduction of gold oxides by AA. To understand and confirm why 1.2 V is an advisable choice to roughen the gold surface, we performed a series of chronoamperometric measurements. Figure 1b shows the current–time transient curves of the gold electrode in 0.5 M AA under different potentials. At a high potential of 1.5 V, the current decreased quickly due to passivation of the gold surface. This passivation phenomenon was also found in the anodization of gold in oxalate [13] and acidic thiourea [17] solutions. While at a low potential of 0.8 V, the current–time transient curve obeyed the Cottrell equation [18, 19] only at the early stage (in 25 s) because of appearance of natural convection soon

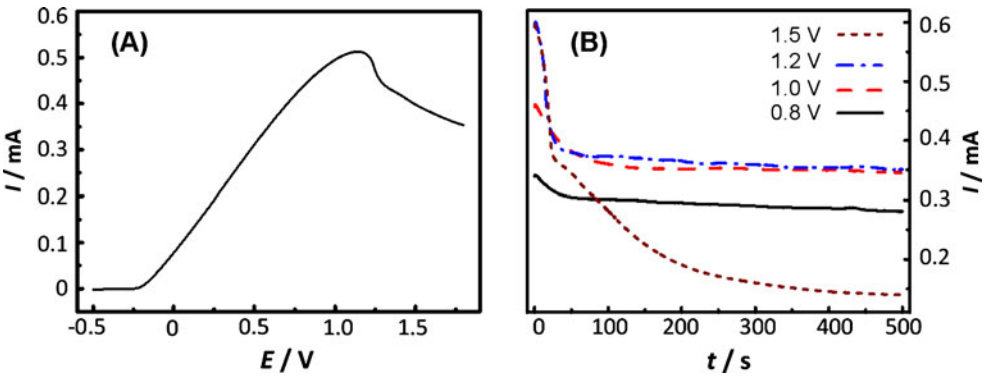

Fig. 1 **a** LSV at 100 mV s^{-1} and **b** the current–time transient curves under different potentials for the gold electrode (1 mm in diameter) in 0.5 M AA

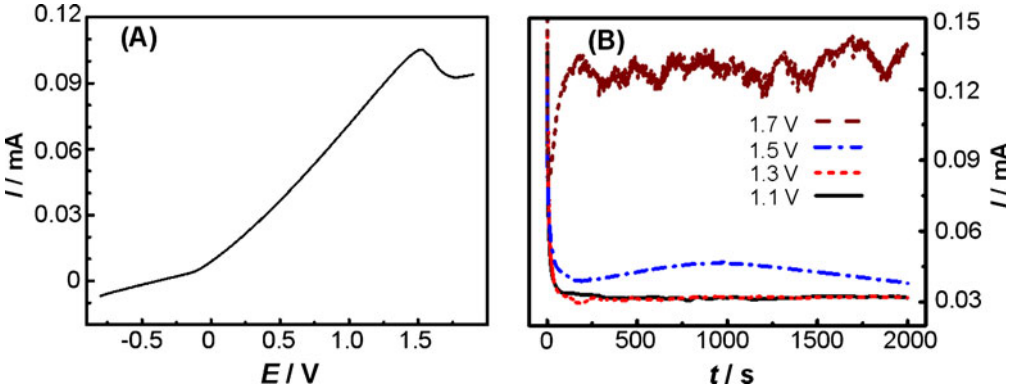

Fig. 2 **a** LSV at 100 mV s^{-1} and **b** the current–time transient curves under different potentials for the gold electrode (1 mm in diameter) in 0.06 M H_2Q

[19]. The current then remained nearly unchanged for the diffusion layer reached a given thickness in the presence of natural convection [19]. It means that the oxidation of AA was the main process at low potentials on the gold electrode and it was governed by the diffusion of AA [20–23]. The oxidations of AA were widely studied on Au, Pt, and mercury electrodes [20–23], and a two-electron transfer was involved in an acidic medium [20]:

$$\mathrm{AA} \rightarrow \mathrm{DHA} + 2e^- + 2\mathrm{H}^+ \quad (1)$$

where AA is L-ascorbic acid and DHA is dehydro-L-ascorbic acid. The current–time curve at 1.2 V in Fig. 1b was distinctive. The initial faradaic current at 1.2 V was as high as that at 1.5 V, indicating that the gold surface was also oxidized into a thin film of gold oxides [24–27] in addition to the oxidation of AA under this moderate potential. The as-formed thin film of gold oxides was then reduced simultaneously and/or subsequently by AA. To the best of our knowledge, AA has been widely used as a reducing agent for the reduction of Au(III) [28, 29]. In view of these facts, the broad current peak around 150 s under 1.2 V in Fig. 1b is temporarily ascribed to the electrocrystallization for gold redox [30–32]. Although there was also a broad current peak around 50 s at 1.5 V in Fig. 1b, the current was too low to fabricate the nano-network gold film effectively due to surface passivation. No such current peak occurred below 1.0 V in Fig. 1b where oxidation of AA was the predominant process.

Similar voltammetric behavior was observed for the gold electrode in the H_2Q aqueous solution as shown in Fig. 2a with a current peak at 1.5 V, and there was also a broad current peak around 1,000 s under 1.5 V in Fig. 2b for the same reason as that peak that appeared at 1.2 V in the solution of AA (Fig. 1b). Processes like oxidation of H_2Q, formation of gold oxide films, reduction of gold oxides by H_2Q, and electrocrystallization due to gold redox were all involved under this potential. Blackening was observed indeed on the gold surface when holding the potential at around 1.5 V, and so 1.5 V was selected here to roughen the gold electrode in H_2Q solution. Differently from AA, strong adsorption of H_2Q on the gold electrode occurred, which was confirmed by SERS in our previous work [33]. H_2Q can be oxidized in the course of adsorption process [34]. At and below 1.3 V in Fig. 2b, the oxidation of gold surface could be effectively depressed due to the strong surface adsorption of H_2Q and its preferential oxidation. While under a high potential of 1.7 V, oxygen gas released displaying apparent noise in the current–time transient curve due to the gas evolution (Fig. 2b).

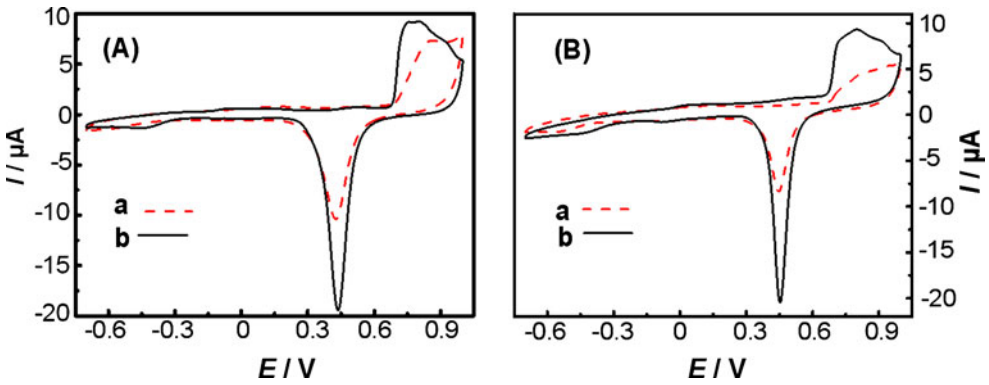

Fig. 3 CVs at 100 mV s^{-1} for the gold electrode in 1 M H_2SO_4 (*a*) before and (*b*) after anodization under **a** 1.2 V for 500 s in 0.5 M AA and under **b** 1.5 V for 2,000 s in 0.06 M H_2Q

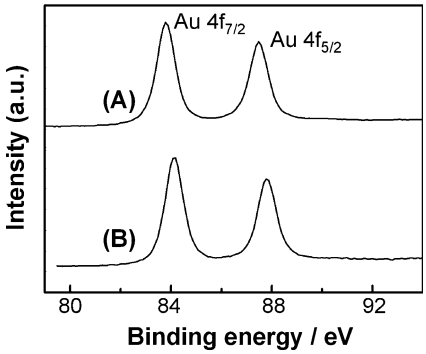

Fig. 4 Au 4f X-ray photoelectron spectra of the gold electrode after anodization under (**a**) 1.2 V for 500 s in 0.5 MAA and (**b**) under 1.5 V for 2,000 s in 0.06 MH_2Q

Characterization of nano-network gold films

Figure 3 shows the cyclic voltammograms (CVs) of the gold electrode in 1 M H_2SO_4 before and after roughening. The real surface area of gold electrodes can be obtained from their CVs by integrating the reduction charge of gold oxide monolayer [34–36], and their roughness factors can be calculated by dividing the real surface area with the geometric surface area of the gold electrode. The roughness factors of the gold electrode before and after anodization under 1.2 V for 500 s in 0.5 MAA were about 3.0 and 6.9 (Fig. 3a), respectively, and the roughness factor was about 6.0 by anodization of the gold electrode under 1.5 V for 2,000 s in 0.06 M H_2Q (Fig. 3b). These results imply that the as-prepared gold nano-network films were of low roughness.

To investigate the surface chemical state of the nano-network film on the gold electrode, X-ray photoelectron spectroscopy (XPS) was carried out. Figure 4 shows the Au $4f_{7/2–5/2}$ XPS of the gold electrode after anodization under 1.2 V for 500 s in 0.5 M AA (A) and under 1.5 V for 2,000 s in 0.06 MH_2Q (B). The doublet peaks of binding energy located at 83.8/87.5 and 84.1/87.8 eV, in consistent well with that of elemental Au(0) (84.0/87.7) [13, 27]. Peaks for trivalent Au(III) (86.4/90.1 eV) or monovalent Au(I) (85.6/89.1 eV)[27, 37] did not appear for both of the nano-network films fabricated in AA and H_2Q solutions.

Figure 5 shows the morphology change of gold electrode surfaces with the increasing anodization time. Small gold nanoparticles of 20–30 nm began to form after anodization for 100 s (Fig. 5a). The amount of gold nanoparticles increased and aggregated into a nano-network film by anodization for about 500 s besides some scattered spherical gold nanoparticles about 100 nm above the film (Fig. 5b, d). Prolonging the anodization to about 1,000 s, the film was replaced by more and larger spherical nanoparticles. From sparsely scattered smaller spheres (~100 nm; Fig. 6a) to densely packed larger particles (~200 nm; Fig. 6c), the morphology evolution also underwent a mid-stage of a nano-network film (Fig. 6b,

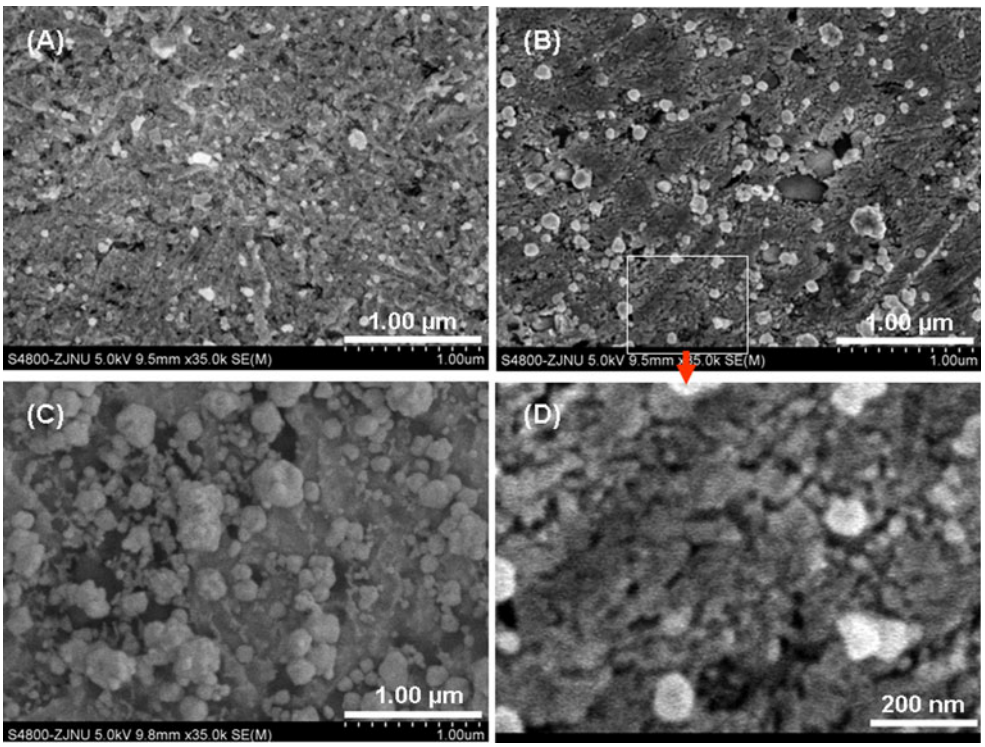

Fig. 5 SEM images of the gold electrode after anodization under 1.2 V in 0.5 M AA for **a** 100 s, **b** 500 s, and **c** 1,000 s. **d** Magnification of the squared area indicated in **b**

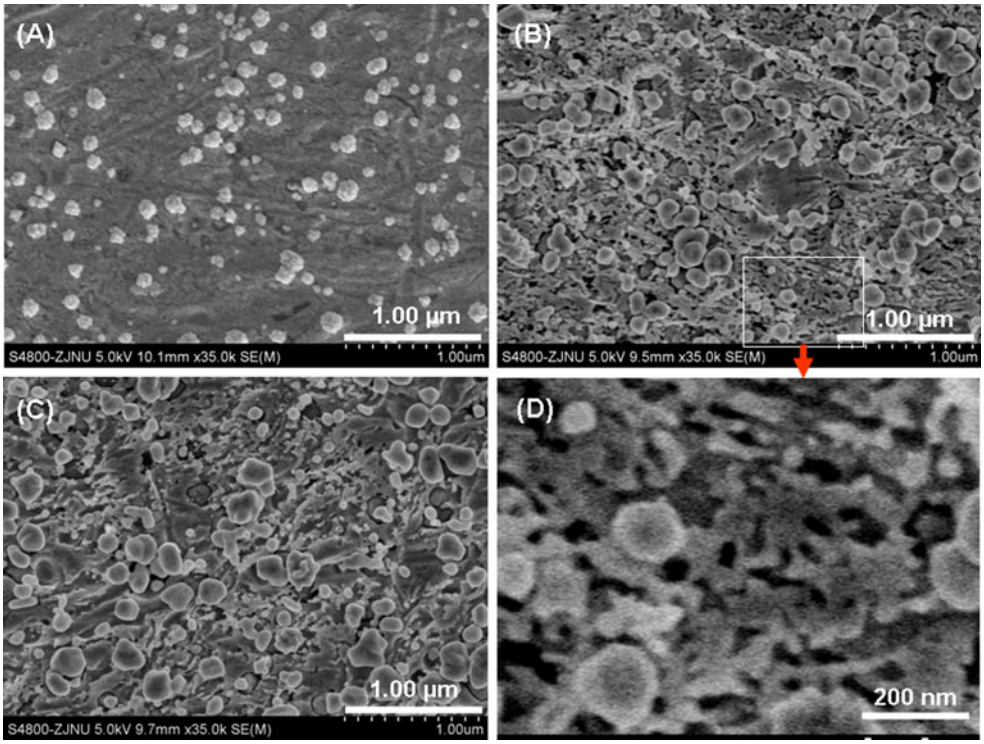

Fig. 6 SEM images of the gold electrode after anodization under 1.5 V in 0.06 M H_2Q for **a** 500 s, **b** 2,000 s, and **c** 3,000 s. **d** Magnification of the squared area indicated in **b**

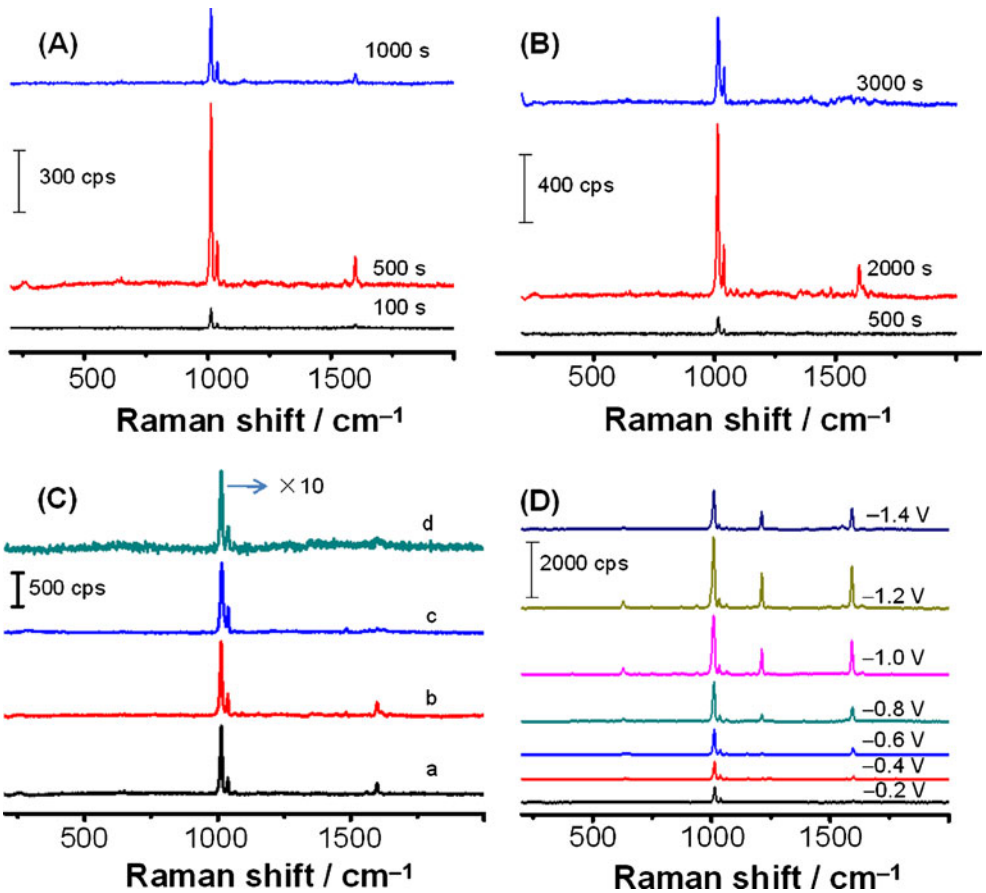

Fig. 7 SERS spectra of Py on the gold electrode after anodization **a** under 1.2 V in 0.5 M AA and **b** under 1.5 V in 0.06 MH_2Q for different times or **c** after different roughening treatments: (*a*) as in **a** for 500 s, (*b*) as in **b** for 2,000 s, (*c*) by potential step to 0.9 V for 50 s in 2 MHCl, and (*d*) by ORC in 0.1 MKCl, or **d** under electrochemical conditions on the gold electrode of Fig. 5**b**

d) during the anodization of gold electrode under 1.5 V in 0.06 M H_2Q.

SERS activity of nano-network gold films

Figure 7a, b shows that the nano-network gold film fabricated in the AA solution for 500 s (Fig. 5b, d) or in the H_2Q solution for 2,000 s (Fig. 6b, d) was optimum for SERS using Py probe molecules (see the ring breathing (ν_1) at 1,014 cm^{-1} [1]) compared with other nanostructures obtained here by anodization of gold in AA or H_2Q solution for different times. These facts imply that the strong SERS effects depend much more on the nanogaps in the nano-networks than on the nano-junctions between the film and the large individual gold nanoparticles. In our previous work [38], purely network-like nanoporous gold films assembled at the air–water interface also showed very strong SERS activity using Py probe molecules, confirming that nanogaps in nano-networks play the key role in the huge enhancement [4, 39, 40].

We are pleased by the comparison results of SERS intensity on the nano-networks here and on the best substrates we could prepare by other electrochemical methods such as newly developed potential step [8–10] and the classical ORC [7]. It has been demonstrated that the enhancement factor on the substrate prepared by the potential step for 50 s in 2 M HCl was 23.3 times as high as that on a commercially available single-use SERS substrate Klarite™ [10]. As shown in Fig. 7c, SERS intensities on the nano-network films fabricated in the AA (a) or H_2Q solution (b) reach to the same absolute value as that on the substrate prepared by the potential step (c) and exceed over that on the substrate prepared by ORC (d). The relative enhancement factors per Py molecule (the absolute intensity divided by the roughness factor) on the nano-network films are roughly five and ten times larger than that on the substrates prepared by potential step and by ORC, respectively. Note that the roughness factor of gold electrode prepared by potential step for 50 s in 2 M HCl was about 35 [10, 16], five times larger than that of nano-network films, and the roughness factor prepared by ORC was about 5, equivalent to that of the nano-networks.

To determine the enhancement factor (EF) of nano-network gold films, the equation proposed by Cai [41] et al. has been used:

$$\mathrm{EF} = \frac{I_{\mathrm{surf}}/N_{\mathrm{surf}}}{I_{\mathrm{bulk}}/N_{\mathrm{bulk}}} \approx \frac{hcN_{\mathrm{A}}\sigma I_{\mathrm{surf}}}{RI_{\mathrm{bulk}}} \quad (2)$$

where h is the effective layer depth within which each Py molecule yields the same contribution to the Raman signal as those localized in the ideally focused plane, c is the concentration of Py, N_A is the Avogadro constant, σ is the surface area occupied by an adsorbed Py molecule, I_{surf} and I_{bulk} denote the integrated intensities of the same ν_1 band for Py that was adsorbed at the surface and that was dissolved in the solution, respectively, and R is the roughness factor of nano-network gold films. Here h is calculated to be 22 μm. According to literature [42], the value of σ is estimated to be 0.27 nm^2; R values for nano-network gold films fabricated in the AA solution for 500 s (Fig. 5b, d) or in the H_2Q solution for 2,000 s (Fig. 6b, d) are 6.9 and 6.0, respectively. The integrated intensities of the bands of ring breathing mode (ν_1) for I_{surf} (1,014 cm^{-1}) are 9,369.47 and 9,371.66 cps for the nano-networks in Figs. 5b, d and 6b, d, respectively. The I_{bulk} of ν_1 (1,005 cm^{-1}) is 0.28 cps. Thus, the EF values for the abovementioned nano-network gold films are calculated to be about 1.69×10^5 and 1.90×10^5, respectively.

The nano-network gold film fabricated directly on the gold electrode surface can be used to investigate SERS behavior conveniently under electrochemical conditions [5]. Figure 7d displays representative potential-dependent SERS spectra of adsorbed Py on that film electrode of Fig. 5b. With negative potential shift, the bands at 1,014 (ν_1) and 1,038 (ν_{12}) cm^{-1} moved to low wavenumbers of 1,008 and 1,032 cm^{-1}, respectively, and the bands at 628 (ν_{6a}), 1,213 (ν_{9a}), and 1,599 (ν_{8a}) cm^{-1} appeared or were enhanced. All the peaks reached the largest intensities at −1.2 V. These results are consistent with previous reports [5].

Conclusions

Nano-network gold films can be prepared via anodization of gold electrodes in an aqueous solution of AA or H_2Q by controlling the applied potential and the anodization time. The production of gold oxide layer by anodization of gold and its simultaneous and/or subsequent reduction by AA or H_2Q are involved in the formation of the nano-network film. The as-fabricated nano-network gold films show very strong SERS activity in comparison with the substrates by some other electrochemical roughening methods.

Acknowledgements We are grateful for the financial supports of this research from Natural Science Foundation of Zhejiang Province of China (Grant No. Y4090658), Open Foundation of Key Laboratory of the Ministry of Education for Advanced Catalysis Materials & Zhejiang Key Laboratory for Reactive Chemistry on Solid Surfaces (Grant No. DH201001), Ph.D. Programs Foundation of the Education Ministry of China (Grant No. 20104306110003), Aid Program for Science and Technology Innovative Research Team in Higher Educational Institutes of Hunan Province, and National Natural Science Foundation of China (Grant Nos. 21173075, 20673103 and 21003045).

References

1. Szamocki R, Reculusa S, Ravaine S, Bartlett PN, Kuhn A, Hempelmann R (2006) Angew Chem Int Ed 45:1317–1321
2. Xia Y, Huang W, Zheng JF, Niu ZJ, Li ZL (2011) Biosens Bioelectron 26:3555–3561
3. Ge XB, Wang RY, Liu PP, Ding Y (2007) Chem Mater 19:5827–5829
4. Ko H, Singamaneni S, Tsukruk VV (2008) Small 4:1576–1599
5. Wu DY, Ren B, Tian ZQ (2008) Chem Soc Rev 37:1025–1041
6. Liu YC, Wang CC, Tsai CE (2005) Electrochem Commun 7:1345–1350
7. Gao P, Gosztola D, Leung LWH, Weaver MJ (1987) J Electroanal Chem 233:211–222
8. Peng YD, Niu ZJ, Huang W, Chen S, Li ZL (2005) J Phy Chem B 109:10880–10885
9. Chu YP, Chen S, Zheng JF, Li ZL (2009) J Raman Spectrosc 40:229–233
10. Gloria D, Justin Gooding J, Moran G, Brynn Hibbert D (2011) J Electroanal Chem 656:114–119
11. Huang W, Wang MH, Zheng JF, Li ZL (2009) J Phy Chem C 113:1800–1805
12. Abdelsalam ME, Bartlett PN, Baumberg JJ, Cintra S, Kelf TA, Russell AE (2005) Electrochem Commun 7:740–744
13. Nishio K, Masuda H (2011) Angew Chem Int Ed 50:1603–1607
14. Nishio K, Masuda H (2010) US Pat 20100230287
15. Kruszewski S (1994) Surf Interface Anal 21:830–838
16. Deng YP, Huang W, Chen X, Li ZL (2008) Electrochem Commun 10:810–813
17. Zhang HG, Ritchie IM, Brooy SRL (2001) J Electrochem Soc 148:D146–D153
18. Lee JW, Pyun SI (2005) Electrochem Acta 50:1777–1805
19. Bard AJ, Faulkner LR (2001) Electrochemical methods, fundamentals and applications, 2nd edn. Wiley, New York
20. Xing X, Shao M, Hsiao MW, Adzic RR, Liu CC (1992) J Electroanal Chem 339:211–225
21. Ruiz JJ, Aldaz A, Dominguez M (1977) Can J Chem 55:2799–2806
22. Rueda M, Aldaz A, Sanchez-Burgos F (1978) Electrochem Acta 23:419–424
23. Březina M, Koryta J, Loučka T, Maršíková D, Pradáč J (1972) J Electroanal Chem 40:13–17
24. Conway BE (1995) Prog Surf Sci 49:331–452
25. Labuda A, Hausen F, Gosvami NN, Grütter PH, Lennox RB, Bennewitz R (2011) Langmuir 27:2561–2566
26. Dickinson T, Povey AF, Sherwood PMA (1975) J Chem Soc, Faraday Trans 1 71:298–311
27. Zhao W, Xu JJ, Shi CG, Chen HY (2006) Electrochem Commun 8:773–778
28. Sun K, Qiu JX, Liu JW, Miao YQ (2009) J Mater Sci 44:754–758
29. Sau TK, Pal A, Jana NR, Wang ZL, Pal T (2001) J Nanopart Res 3:257–261
30. Schultze JW, Lohrengel MM (1976) Ber Bunsen-Ges Phys Chem 80:552–556
31. Schultze JW, Lohrengel MM, Ross D (1983) Electrochim Acta 28:973–984
32. Ferro CM, Calandra AJ, Arvía AJ (1975) J Electroanal Chem 65:963–988
33. Xu YZ, Zhang YR, Zheng JF, Guo C, Niu ZJ, Li ZL (2011) Int J Electrochem Sci 6:664–672
34. Laviron E (1984) J Electroanal Chem 164:213–227
35. Trasatti S, Petrii OA (1991) Pure Appl Chem 63:711–734
36. Rand DAJ, Woods R (1971) J Electroanal Chem 31:29–38
37. Sylvestre JP, Poulin S, Kabashin AV, Sacher E, Meunier M, Luong JHT (2004) J Phy Chem B 108:16864–16869
38. Wang MH, Chen S, Xia Y, Zhang YR, Huang W, Zheng JF, Li ZL (2010) Langmuir 26:9351–9356
39. Park WH, Ahn SH, Kim ZH (2008) ChemPhysChem 9:2491–2494
40. Tong LM, Zhu T, Liu ZF (2011) Chem Soc Rev 40:1296–1304
41. Cai WB, Ren B, Li XQ, She CX, Liu FM, Cai XW, Tian ZQ (1998) Surf Sci 406:9–22
42. Stolberg L, Lipkowski J, Irish DE (1990) J Electroanal Chem 296:171–189